Results in Physics 10 (2018) 427–433

Contents lists available at ScienceDirect

Results in Physics

journal homepage: www.elsevier.com/locate/rinp

Experimental study on the interfacial shear stress of RC beams strengthened with prestressed BFRP rod

Qiaoyun Wu[a], Shiye Xiao[a], Kentaro Iwashita[b,*]

[a] School of Civil Engineering and Architecture, Wuhan Institute of Technology, Wuhan 430073, China
[b] Department of Civil Engineering, Meijo University, 1-501 Shiogamaguchi, Tempaku-ku, Nagoya 468-8502, Japan

ARTICLE INFO

Keywords:
Basalt fiber reinforced polymer (BFRP) rod
Interfacial shear stresses
Maximum achievable prestress level
Strengthening
Debonding

ABSTRACT

On the strengthening of concrete structures by externally bonding prestressed BFRP (basalt fiber reinforced polymer) rod, the release of the prestress may cause an interfacial shear stress concentrated at the prestressed BFRP ends which may cause BFRP prematurely debonding. In order to avoid this problem, the shear stress caused by BFRP prestress should not exceed the interfacial adhesive strength. In this study, the mechanical properties of the adhesive interface at the ends of the BFRP rod which is bonded to the concrete beams are evaluated by experimental studies considering different test methods such as the stretch adhesion test at both ends (double pull-pull test) and prestressed import test (single push-push test). Based on the existing research results, a modified formula is derived to predict the interfacial shear stresses, BFRP stresses and maximum achievable prestress level. The accuracy and validity of the proposed theoretical formula are confirmed by the experimental results. Moreover, an effective method of decreasing the interfacial shear stress is proposed for avoiding the possible premature failure near the BFRP ends caused by the shear stress concentration.

Introduction

Strengthening of reinforced concrete structures by externally bonding FRP sheets is a new, fast and effective strengthening technique which has been widely studied and applied at home and abroad in recent years. At present, the most widely used fiber types in the field of building and bridge reinforcement are CFRP (carbon fiber reinforced polymer), GFRP (glass fiber reinforced polymer) and AFRP (aramid fiber reinforced polymer). One of the commonly used is the CFRP whose comprehensive performance is the best. However, the expensive price hinders its wide application. Although the GFRP and AFRP are inexpensive, the gap with CFRP is significant in terms of mechanical properties and extended durability.

The BFRP (basalt fiber reinforced polymer) with high strength, good durability and cost advantages has become a hot material in the field of civil engineering reinforcement [1–5]. The strengthening technique of adhering BFRP sheets, which is applied by prestress, to the concrete surface with epoxy resin is being developed and applied to civil engineering field. In general, when the continuous fiber cloth is bonded to the concrete surface, the soaked low viscosity epoxy resin is always used [6–8]. During the past research, the strengthening materials are generally BFRP sheets and there is less research on the interfacial shear stress at the bonding end. Lu et al. [9] studied the long-term durability of BFRP sheets and the epoxy resin matrix in a wet-dry cyclic environment containing chloride ions. Qin et al. [10] presented the results of testing reinforced concrete beams strengthened with the BFRP sheets. Jiang et al. [6] proposed a repair technique using near-surface-mounted (NSM) basalt fiber reinforced polymer (BFRP) bars and BFRP sheets jacketing, and then four one-fourth scale earthquake-damaged reinforced concrete circular bridge columns repaired by the proposed technique were retested under the similar cyclic lateral load as the corresponding original columns. Ibrahim et al. [11] presented the seismic performance of concrete bridge columns reinforced with both steel and fiber-reinforced polymer. Wu et al. [12] evaluated the residual tensile properties of unstressed and stressed BFRP bars exposed to four types of simulated harsh environments. Ramaswamy et al. [13] dealt with the behavior of basalt fiber reinforced polymer (BFRP) composites retrofitted RCC piles subjected to axial compression loads. Yao et al. [14] presented an analysis of the seismic performance of square RC bridge columns retrofitted with near-surface-mounted (NSM) basalt fiber-reinforced polymer (BFRP) bars and/or BFRP sheet confinement based on fiber element modeling.

In this paper, the experimental study of the BFRP rod with high viscosity epoxy resin bonded to the concrete surface is carried out. The reasons or the advantages of using BFRP rod as the strengthen material are (1) In most previous studies, BFRP sheet is always used as the

* Corresponding author.
E-mail address: iwak@meijo-u.ac.jp (K. Iwashita).

https://doi.org/10.1016/j.rinp.2018.06.007
Received 7 March 2018; Received in revised form 4 June 2018; Accepted 4 June 2018
Available online 20 June 2018

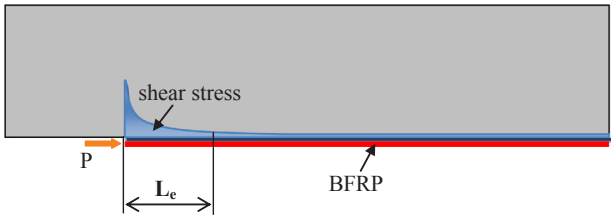

Fig. 1. Distribution of the shear stress at the bonding end.

strengthen material, and little studies are focus on the BFRP rod; (2) When BFRP rods is used as the strengthen material, it is very convenient to apply prestress to improve the strengthen effect.

The templates are installed around the BFRP rod and high viscosity epoxy is injected into the templates, bonding the BFRP rod to the surface of the concrete beams. Using post-tension method, the BFRP rod is prestressed. After the adhesive material has been hardened, rapidly release the prestress and at this time, the excellent shear stress is developed at the bonding end, as shown in Fig. 1 where P is the released prestress and L_e is the effective bonding length, which will cause the possibility of early debonding. The evaluation of the shear stress and the improvement of the bonding strength have become an important issue. In view of this, the experiments of the bonding end of the prestressed BFRP rod by loading different forces are carried out. According to Fig. 2, the applicability of the tensile test at the bonding end is verified. Based on the knowledge of the proposed bonding measures of the adhesive interface of FRP and concrete, a new conditional condition for not allowing the adhesive end to be peeled off is proposed. Moreover, an effective method of decreasing the interfacial shear stress is proposed which is discussed experimentally as well.

The proposal of the condition for not allowing the adhesive end to be peeled off

The BFRP rod is bonded to the surface of a concrete beam, as seen in Fig. 2. In the experiment of tearing off the BFRP rod, referring to previous studies by Wu [15], the relationship between the shear stress τ and the slip δ can be represented by the elastic-peel model which is shown in Fig. 3 where the slop k_s is the section stiffness and τ_u is the maximum shear stress. The area surrounded by the model curve and the δ axis is known as the interface stripping damage energy G_f. The elastic model of the relationship between the shear stress τ and the slip δ not only simplifies the theoretical derivation process but also gets accurate results.

Referencing to Wu [15], it has

$$\tau_u = \sqrt{2G_f k_s} \tag{1}$$

The maximum shear stress generated at the bonding end according to the imported prestress can be calculated referencing to Niu [16]

$$\tau_{\max} = \sigma_p \sqrt{\frac{k_s t_f}{E_f}} \tag{2}$$

where t_f is the thickness of BFRP sheet and E_f is the elasticity modulus of the BFRP. In order to prevent the debonding of the BFRP, the τ_u in Eq.

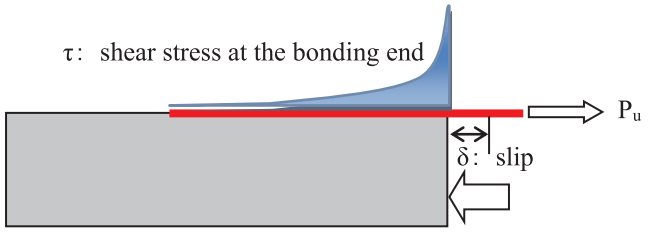

Fig. 2. Adhesive test schematic diagram.

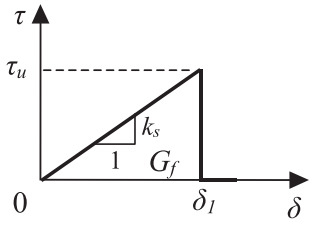

Fig. 3. Relationship between the shear stress τ and the slip δ (elastic-peel model).

(1) should smaller than $\tau_{\max}$ in Eq. (2). The available of the applied prestress σ_p is

$$\tau_u > \tau_{\max} \rightarrow \sqrt{2G_f k_s} > \sigma_p \sqrt{\frac{k_s t_f}{E_f}} \rightarrow \sigma_p < \sqrt{\frac{2G_f E_f}{t_f}} \tag{3}$$

Theoretical study on the concentrate shear stress at the bonding end

As the calculation methods for the shear strength of the bonding interface between BFRP and the concrete, the Katahiki adhesion test (prestress imported test) and Ryohiki adhesion test (stretch adhesion test at both ends) are commonly used in the stretching test of the bonding end [17–21]. Thus, through the tensile and compression experiments of the bonding end, the theoretical formulas of each shear stress distribution are compared, and the applicability of each test is verified. The reinforcement beam with prestressed continuous BFRP and the deformation of the X-X cross section of the concrete beam which is externally bonded by prestressed BFRP are shown in Fig. 4(a) and (b) according to the proposal of Niu [16]. In addition, the X-X cross section means that the predetermined prestress is fully implemented. Due to the introduction of the prestress, the concrete beam is compressed, and the amount of compression is bigger than the BFRP. Therefore, there is a relative slip δ between the lower end of the compressed concrete beam of the X-X cross section and the compressed BFRP. According to the slip δ and the shear stress τ, Niu [16] proposed the shear stress distribution formula $\tau(x)$ of the bonding end which is listed in Eq. (4)

$$\tau(x) = \sigma_p \sqrt{\frac{\tau_u^2}{2G_f E_f} \frac{t_f}{(1+\alpha t_f)}} \frac{\sinh(\beta_1 x)}{\cosh(\beta_1 l)} \tag{4}$$

in which

$$\alpha = \frac{E_f b_f}{E_c}\left(\frac{1}{b_c t_c} + \frac{t_n^2}{I_c}\right), \quad \beta_1 = \sqrt{\frac{k_s}{E_f t_f}} \tag{5}$$

where σ_p is the imported prestress (N/mm^2), τ_u is the maximum shear stress (N/mm^2), t_f is the thickness of BFRP sheet (mm), G_f is the interface stripping damage energy (N/mm) and E_f is the elasticity modulus of the BFRP (N/mm^2), l is the length from the bonding end of the BFRP to the middle of the span (mm), b_f is the width of the BFRP (mm), E_c is the elasticity modulus of the concrete beam (N/mm^2), b_c is the width of the concrete beam (mm) and t_c is the height of the concrete beam (mm), t_n is distance of the cross section from the axis to the lower flange (mm), I_n is the second moment of the area (mm^4), α is the coefficient considering the ratio of section stiffness of BFRP to concrete beam and the moment caused by the importing of prestress and when the section of the concrete beam is very large, it has $\alpha = 0$. Thus, Eq. (4) can be replaced by Eq. (6)

$$\tau(x) = \sigma_p \sqrt{\frac{\tau_{\max}^2 t_f}{2G_f E_f}} \frac{\sinh(\beta_1 x)}{\cosh(\beta_1 l)} = \sigma_p \sqrt{\frac{k_s t_f}{E_f}} \frac{\sinh(\beta_1 x)}{\cosh(\beta_1 l)} \quad \left(\beta_1 = \sqrt{\frac{k_s}{E_f t_f}}\right) \tag{6}$$

So there is

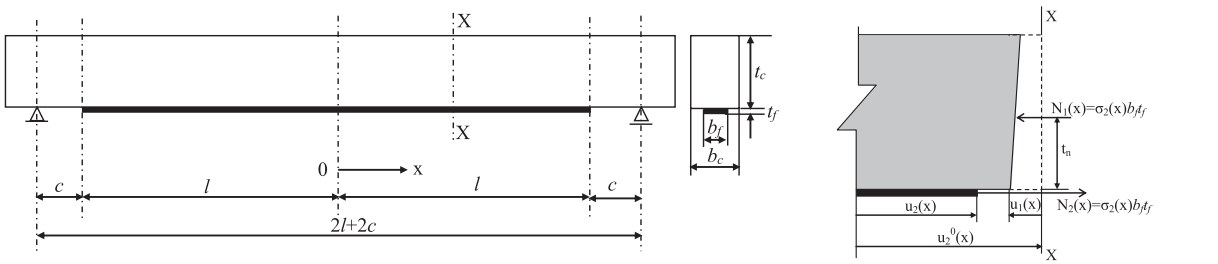

(a) Reinforcement beam with prestressed continuous BFRP

(b) The deformation of the X-X cross section after implied prestress

Fig. 4. The concrete beam of the prestress imported test.

$$\tau(x) = \sigma_p\sqrt{\frac{k_s t_f}{E_f}}\frac{\sinh(\beta_1 x)}{\cosh(\beta_1 x)}\cdot\frac{\cosh(\beta_1 x)}{\cosh(\beta_1 l)} = \sigma_p\sqrt{\frac{k_s t_f}{E_f}}\tanh(\beta_1 x)\cdot\frac{\cosh(\beta_1 x)}{\cosh(\beta_1 l)} \tag{7}$$

By Eq. (2), Eq. (7) can be replaced by Eq. (8)

$$\tau(x) = \tau_{\max}\tanh(\beta_1 x)\frac{\cosh(\beta_1 x)}{\cosh(\beta_1 l)} \tag{8}$$

On the other hand, the distribution of shear stress of $\tau'(x)$ referencing to the research of Wu [21,19] is theoretically represented by Eq. (9) in the stretch adhesion test at both ends

$$\tau'(x) = \tau_{\max}\frac{\cosh(\lambda x)}{\cosh(\lambda l)} \quad \left(\lambda = \sqrt{\frac{k_s}{E_f t_f}}\right) \tag{9}$$

By Eqs. (8) and (9), it has

$$\tau(x) = \tanh(\beta_1 x)\tau'(x) \tag{10}$$

Therefore, the shear stress $\tau(x)$ produced at the bonding end in stretch adhesion test is obtained by $\tau'(x)$ multiplying by $\tanh(\beta_1 x)$. In addition, in the prestressed import test, the shear stress $\tau(x)$ produced at the bonding end is expressed by the similar calculation, which theoretically indicates that using the stretch adhesion test at both end can evaluate the shear stress produced at the bonding end in prestressed import test.

Experimental study on the shear stress of bonding end

Details of the experimental model and the experimental method

In the previous section, the shear stress concentrated on the bonding end in stretch adhesion test and prestressed import test is theoretically explored. The experimental discussion is carried out in this section. The experimental model as shown in Fig. 5 is an RC beam which is imported by prestressing. The cross section of the RC beam is 100 mm × 150 mm and the length is 600 mm. Four steel bars of 6 mm in diameter are equipped which insure that the RC beam will not produce cracks even if the prestressing is imported. Firstly, polishing the surface of the concrete so that the aggregate is exposed (see Fig. 6(b)). In order to flatten the bonding interface on the surface of the experimental model, the epoxy primer is coated. Then, placing a 10 mm BFRP bar which is prestressed on the epoxy primer, surrounded by a template with a height of 20 mm, width of 50 mm and length of 600 mm. Finally, the template is filled with epoxy resin. The physical properties of each material tested by the uniaxial tensile experiment is listed in Table 1. In order to explore the improvement measures for increasing the shear stress, before pasting the prestressed BFRP rod, it pasted a BFRP sheet as the first testing and the effectiveness for additionally pasting the BFRP sheet will be discussed in Section "Discussions of the experimental results of increasing the maximum shear stress at the bonding end". The prestressed import test model is plotted in Fig. 6.

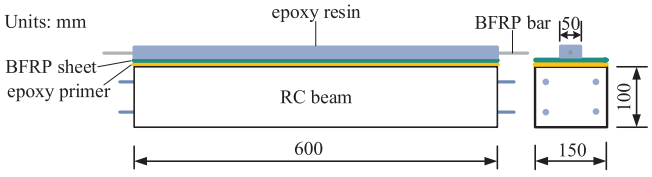

Fig. 5. The experimental model in the prestressed import test.

On the other hand, the testing models of the stretch adhesion test at both ends are shown in Fig. 7(a) and (b). The section size of the testing model is 150 mm × 200 mm, and the length is 300 mm. Two BFRP bars are bonded to both sides of the concrete testing model in the same manner as described above. The height and width of the epoxy coating are 20 mm and 25 mm, respectively. A steel bolt with the diameter of 24 mm is fully embedded into the middle of the concrete model to ensure adequate adhesion. As shown in Fig. 7, the BFRP rod is stretched in the opposite direction by filling the expanded cement into the fixed steel pipe which located at one side end of the BFRP rod. At this time, the shear force is generated at the bonding surface between the BFRP rod and the concrete model. The Yong's modulus and thickness of the BFRP rod (the cross-sectional area of the BFRP rod divided by the bond width as the thickness) and the cross-section stiffness (referencing to the research of Wu [2], the stiffness is tentatively set by 160 N/mm^3) are substituted into the previous section of Eq. (6), so $\tanh(\beta_1 x)$ $(x = 300$ mm$)$ can be calculated as: $\beta_1 = \sqrt{k_s/(E_f t_f)} = \sqrt{160/[90000 \times (51/20)]} = 0.0264$, $\tanh(\beta_1 x) = \tanh(0.0264 \times 300) \approx 0.99999$. Therefore, the maximum shear stress in the prestressed import test and the stretch adhesion test at both ends of this study is theoretically the same according to Eq. (10) as $\tau(x) \approx \tau'(x)$.

Test results and discussions

The failure modes of the two test specimens are shown in Fig. 8. During the loading process of the prestressed imported test, the final failure mode is the yielding of the reinforcement in the tensile area and the BFRP rod stripping from the concrete surface and then the concrete of the compressive region is crushed. The failure mode is displayed in Fig. 8(a). For the stretch adhesion test, the final failure mode is that the BFRP rods are only bilateral stripped at one end of the test specimen which is brittle failure as plotted in Fig. 8(b).

Tables 2 and 3 list the test datum of the two experimental models, where P is the maximum load, ε is the maximum strain, μ is the strain of the model at different distances from the bonding end, $\tau_{\max}$ is the maximum shear stress, δ is the slippage between two survey points, ΔG_f is the stripping destructive energy between tow survey points and G_f is the total stripping destructive energy. τ_i is calculated by different strain values between tow survey points and the physical properties (such as the Yong's Modulus and cross section area of each material) of each testing material which is listed in Table 1, and the maximum value of τ_i

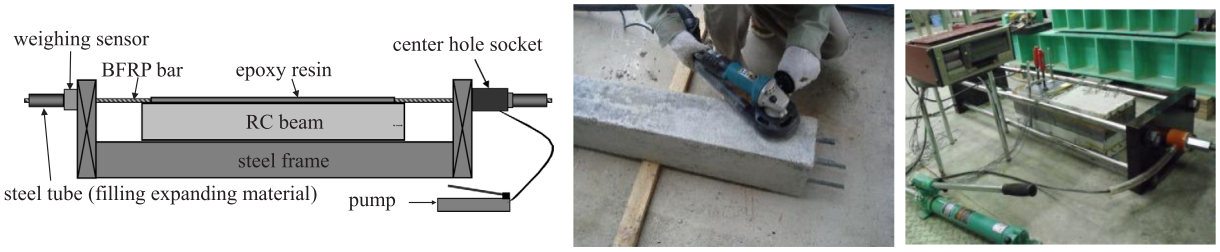

(a) Schematic diagram (b) Test figures

Fig. 6. The prestressed import test model.

Table 1
The physical properties of each material.

Yong's Modulus of elasticity for tension of epoxy resin E_a (N/mm^2)	4600	
Yong's Modulus of elasticity for tension of BFRP E_f (N/mm^2)	90,000	
Tensile strength of BFRP bar $_f$ (N/mm^2) (theoretical value)	1251	
Fiber content of BFRP bar (%)	65	
Cross section area of one BFRP bar A_f (mm^2)	Area of BFRP A_{ff}	51.0
	Area of epoxy resin A_{fa}	27.5
Cross section area of the epoxy resin formed outside the BFRP bar A_a (mm^2)	Prestressed import test	949.0
	Stretch adhesion test at both ends	398.0
Concrete compressive strength of maintenance for 28 days (N/mm^2)	20.5	

under different survey points and the same maximum load P is τ_{max}. δ is calculated by the algebraic operation of strain values at each survey point. ΔG_f is calculated by the product of τ_{max} and δ while the relationship between τ_{max} and δ is former plotted in Fig. 3. Therefore, the total stripping destructive energy G_f is calculated to be 0.37 N/mm for the prestressed import test and 0.39 N/mm for the stretch adhesion test as listed in Tables 2 and 3, respectively. The two values are very closer. The total stripping destructive energy in the prestressed import test is 0.95 times (0.37/0.39 = 0.95) of the stretch adhesion test.

The strain distribution curves of the two testing models are displayed in Figs. 9 and 10. It can be seen from Figs. 9 and 10 that, with the increasing of the maximum load the strain of the BFRP rod increases. The farther away from the crack, the smaller of the strain. The maximum strain for the stretch adhesion test (μ = 4315) is larger than the prestressed import test (μ = 2958). For the prestressed import test, when the distance from the crack is less than 40 mm, with the increasing of the distance, the stain of the BFRP rod at maximum load of 14.1 kN and 13.4 kN decreases slowly. However, for the other loading conditions, no matter for the prestressed import test or the stretch adhesion test, with the increasing of the distance from the crack, the stain of the BFRP rod decreases rapidly.

Figs. 11 to 12 show the interfacial shear stress distribution curves at different distances from the bonding end of the two test models. From Fig. 11, it can be seen that, the shear stress has a minimum value at the position of 120 mm far away from the bonding end. When the distance is less than 120 mm, with the decreasing of the distance, the shear stress increases. In addition, the shear stress of the bonding end increases with the increasing of the loading. Fig. 12 shows different laws of curve variation compared with Fig. 11 because of the different loading methods. As shown in Fig. 12, excepting for the maximum loading condition (79.4 kN) which has a minimum shear stress at the distance from the bonding end of 90 mm, the shear stress decreases with the increasing distance from the bonding end. The greater the loading value, the larger of the maximum shear stress at the distance from the bonding end of 30 mm. In addition, as can be seen from Fig. 12 that, the shear stress in the loading condition of 79.4 kN is smaller than that in 71.0 kN. This is because in the stretch adhesion test, the test model has been damaged by the brittle failure when loading to 79.4 kN.

Figs. 13 to 14 show the interfacial shear stress distribution curves at different distances from the crack of the two test models. Fig. 13 plots that, the changing law of the curves is consistent with Fig. 11. The shear stress for different loading conditions has a minimum value at the distance from the crack of 120 mm. From Fig. 14 it can be seen that, when the distance from the crack is less than 150 mm, the shear stress for different loading conditions always increases with the increasing of the distance and then decreases then increases and then decreases, changing like this cycle. From Fig. 14, it also can be seen that the trend of the maximum loading condition (79.4 kN) is very different from other curves (like Fig. 12), especially at the survey point of the distance

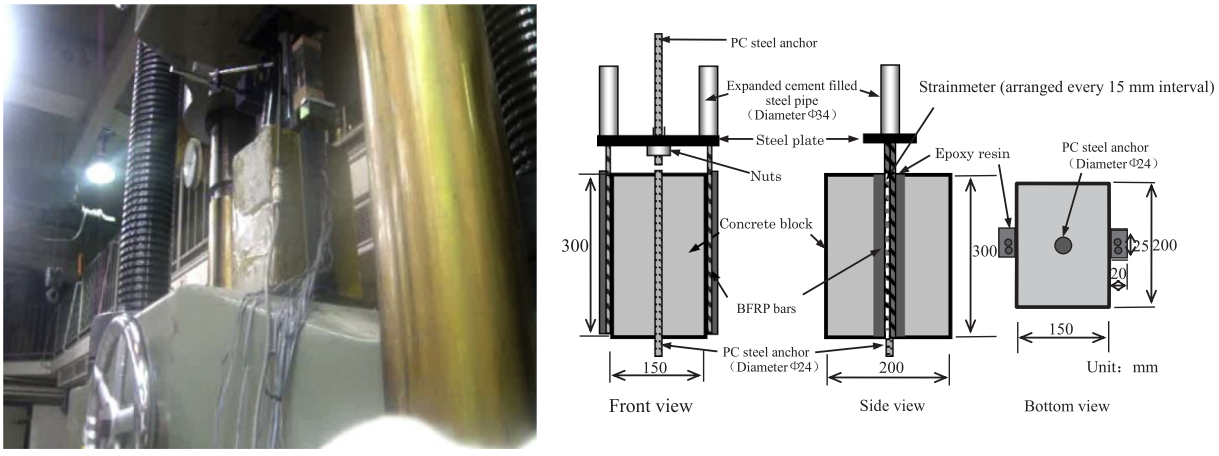

(a) Test figure (b) Schematic diagram

Fig. 7. The stretch adhesion test model.

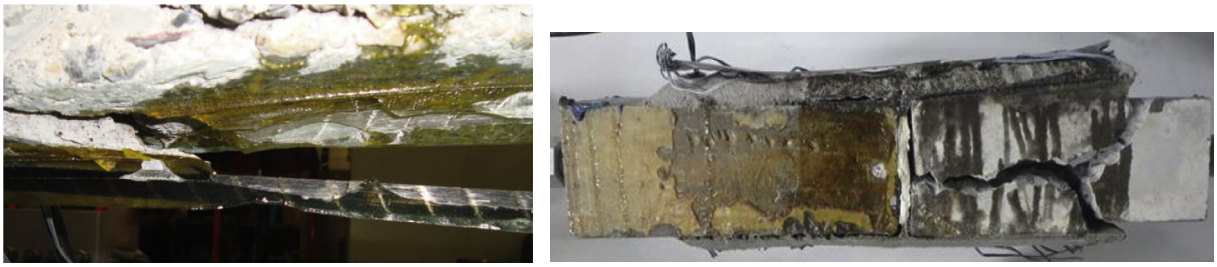

(a) Prestressed import test (b) Stretch adhesion test

Fig. 8. Failure modes of the two test models.

from the crack of 90 mm, the shear stress dropped to the loading condition of 50.7 kN. The reason for the strange distribution for the stretch adhesion test is that when the load increased to 79.4 kN, the specimen suddenly occurred brittle failure damage at the position of 90 mm away from the crack. The similar situation is shown in Fig. 14.

In the prestressed import test, the final stripping state of the BFRP is that, from the bonding end, the concrete surface and the adhesive layer produced an upward curl in an integrated state and then shed stripping. In the stretch adhesion test at both ends, the final stripping state of the BFRP is that, crack peeling occurs at the surface of the concrete near the bonding end. The maximum shear stress in the prestressed import test is 0.8 times (10.53/13.09 = 0.8 as listed in Tables 2 and 3) of the stretch adhesion test. The reason for this deviation is that, in the prestressed import test, the estimated value of the 2-point deformation for getting the maximum shear stress near the pre-crack has a certain error. The total stripping destructive energy is calculated by all strain values measured by the strain gauges, and the calculated value is considered to be relatively stable. Therefore, it is considered that the maximum shear stress and the total stripping destructive energy obtained by the stretch adhesion test are relatively stable.When using the stretch adhesion test to design the shear stress of the bonding end, referencing to $\tanh(\beta_1 x)$ in Eq. (10), it can be considered as the following formula which takes into account the safety factor k_1:

$$\tau_u > \tau_{\max} \rightarrow \tanh(\beta_1 x)k_1\sqrt{2G_f k_s} > \sigma_p\sqrt{\frac{k_s t_f}{E_f}} \rightarrow \sigma_p < \frac{\tanh(\beta_1 x)}{k_1}\sqrt{\frac{2G_f E_f}{t_f}} \tag{11}$$

Here, the thickness of the BFRP is calculated by the cross-sectional area of the basalt fiber and the converted area of the epoxy resin divided by the bonding width. Therefore, the Eq. (11) can be rewritten as Eq. (12):

$$\sigma_p < \frac{\tanh(\beta_1 x)}{k_1}\sqrt{\frac{2G_f E_f}{t_f}} = \frac{\tanh(\beta_1 x)}{k_1}\sqrt{\frac{3G_f E)f}{A_{ff} + n_{fa}(A_{fa} + A_a))/b_f}}, \quad n_{fa} = \frac{E_a}{E_f} \tag{12}$$

Assuming that the safety factor of k_1 is 1, the upper limit of the introduced prestress for the prestressed import test calculated from the above Equation (Eq. (12)) is:

$$= \frac{\tanh\left(\sqrt{\left(\frac{160}{90000\times\left(\left(51.0+\frac{4600}{90000}(27.5+949.0)\right)/50\right)}\right)}\times 300\right)}{\sqrt{\frac{2\times 0.37\times 90000}{\left(51.0+\frac{4600}{90000}(27.5+949.0)\right)/50}}} = 181.67\ \text{N/mm}^2$$

While the measured value for the prestressed import test is 180 N/mm^2 (180/1251 = 14.4% of the tensile strength for BFRP rod) which is very closer to the theoretical value.

Similarly, the upper limit of the introduced prestress for the stretch adhesion test calculated from the Eq. (13) is:

$$\sigma_p < \frac{\tanh(\beta_1 x)}{k_1}\sqrt{\frac{2G_f E_f}{t_f}} = \frac{\tanh\left(\sqrt{\left(\frac{k_s}{E_f\left(\left(A_{ff}+\frac{E_a}{E_f}(A_{fa}+A_a)\right)/b_f\right)}\right)}x\right)}{k_1}\sqrt{\frac{2G_f E_f}{\left(A_{ff}+\frac{E_a}{E_f}(A_{fa}+A_a)\right)/b_f}}$$

$$= \frac{\tanh\left(\sqrt{\left(\frac{160}{90000\times\left(\left(51.0+\frac{4600}{90000}(27.5+398.0)\right)/20\right)}\right)}\times 300\right)}{\sqrt{\frac{2\times 0.39\times 90000}{\left(51.0+\frac{4600}{90000}(27.5+398.0)\right)/20}}} = 138.93\ \text{N/mm}^2 \tag{13}$$

While the measured value for the stretch adhesion test is 135 N/mm^2 (135/1251 = 10.8% of the tensile strength for BFRP rod) which is very closer to the theoretical value, either. Through the comparison between the theoretical and experimental values of the introduced prestress, it proves the applicability of the improved formula proposed in this paper.

Table 2
Measured data (prestressed import test).

P (kN)	ε	Strain μ under different survey points (distance from bonding end)										$\tau_{\max}$ (N/mm^2)	δ (mm)	⊿G_f (N/mm)	G_f (N/mm)
		0	30	45	60	75	90	105	120	195	200				
0	0	0	0	0	0	0	0	0	0	0	0	0.00	0.000	0	0.370
0.8	174	94	56	37	26	19	15	12	11	7	0	0.25	0.001	0.000	
5.7	1241	933	534	345	246	182	152	114	95	11	0	2.26	0.013	0.015	
8.7	1894	1650	892	570	407	299	246	185	153	19	0	3.85	0.021	0.025	
10.1	2199	2017	1151	716	506	369	303	226	184	27	0	5.20	0.026	0.023	
11.6	2525	2415	1532	934	649	470	382	281	228	31	0	7.14	0.034	0.050	
12.3	2678	2579	1759	1074	739	531	429	315	252	35	0	8.18	0.039	0.035	
13.4	2917	2787	2555	1696	1123	774	608	429	334	43	0	10.26	0.055	0.150	
14.1	3070	2958	2872	1990	1302	884	691	486	374	47	0	10.53	0.062	0.072	

Table 3
Measured data (stretch adhesion test).

P (kN)	ε	Strain μ under different survey points (distance from bonding end)										τ_{max} (N/mm^2)	δ (mm)	ΔG_f (N/mm)	G_f (N/mm)
		0	30	45	60	75	90	105	120	135	150				
0	0	0	0	0	0	0	0	0	0	0	0	0.00	0.000	0	0.392
20.6	1121	1050	184	109	70	56	39	32	21	15	7	1.10	0.003	0.002	
30.7	1671	1627	318	183	117	92	62	51	34	23	10	1.98	0.005	0.003	
40.6	2210	2212	485	286	182	143	95	79	52	35	16	2.92	0.007	0.006	
50.7	2760	2823	793	468	297	231	151	125	85	59	33	4.77	0.012	0.018	
60.6	3299	3410	1263	676	446	347	229	190	135	100	61	8.62	0.020	0.049	
71.0	3865	3907	1832	941	631	506	334	279	202	152	93	13.09	0.028	0.096	
79.4	4322	4315	2375	1563	1096	826	545	515	369	277	184	11.93	0.037	0.113	

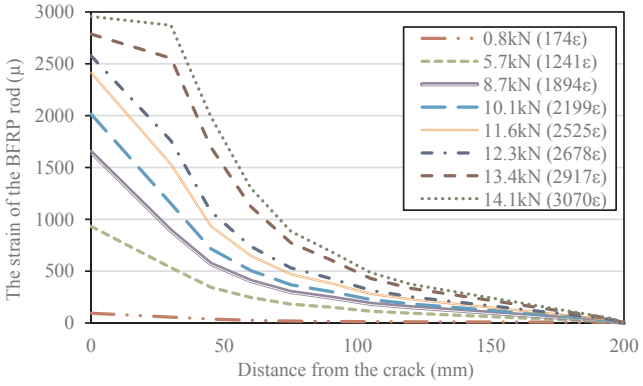

Fig. 9. The distribution of the strain (prestressed import test).

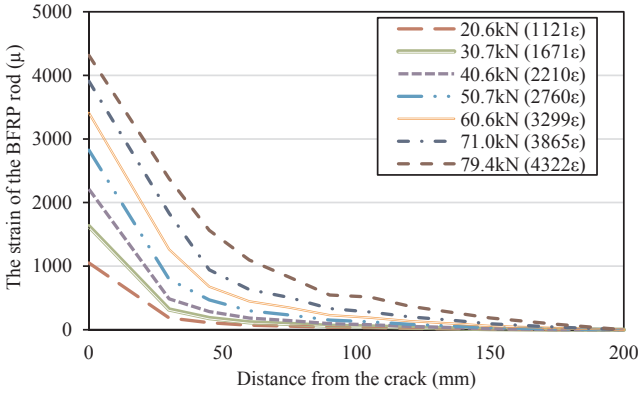

Fig. 10. The distribution of the strain (stretch adhesion test).

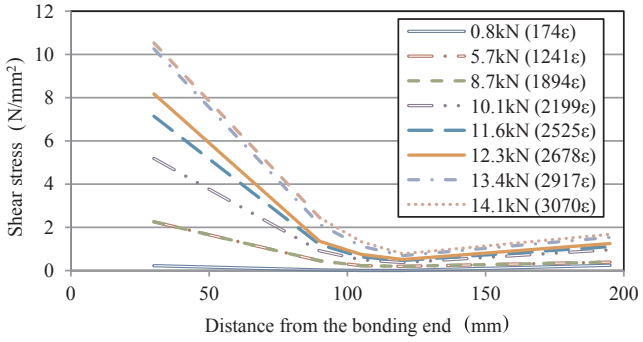

Fig. 11. The distribution of the shear stress under different distances from the bonding end (prestressed import test).

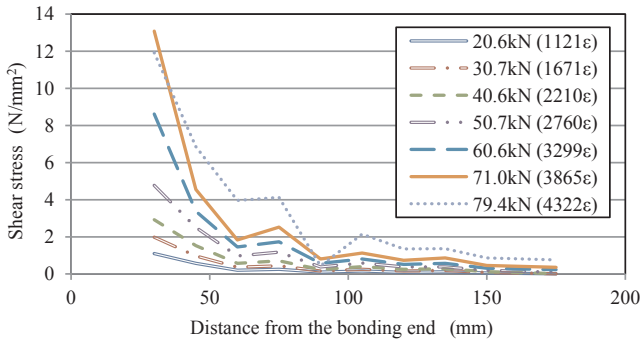

Fig. 12. The distribution of the shear stress under different distances from the bonding end (stretch adhesion test).

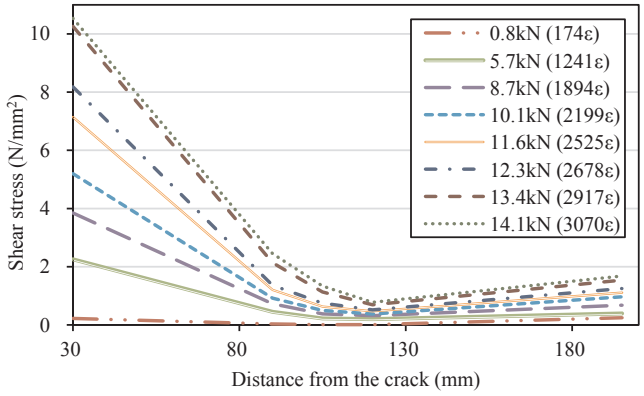

Fig. 13. The distribution of the shear stress under different distances from the crack (prestressed import test).

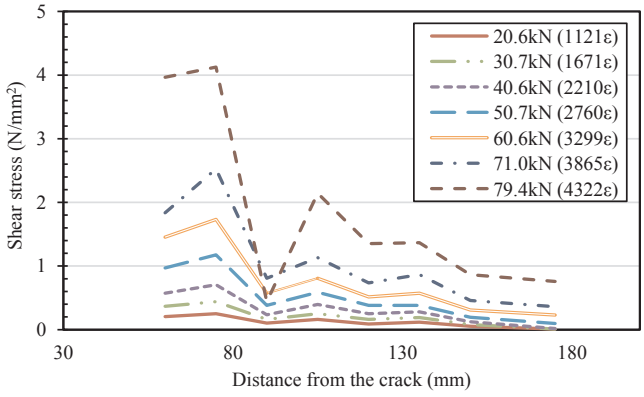

Fig. 14. The distribution of the shear stress under different distances from the crack (stretch adhesion test).

Discussions of the experimental results of increasing the maximum shear stress at the bonding end

Before pasting the prestressed BFRP rod, it pasted a BFRP sheet with a width of 100 mm and thickness of 0.166 mm here. Then, the peel test is carried out using the stretch adhesion test. At this time, the interface between the BFRP rod and the surrounding epoxy resin modeled portion and the BFRP sheet does not peel off. The maximum load is 143.71 kN, which is 1.81 times bigger than the non-paste BFRP sheet (79.4 kN as shown in Figs. 10, 12 and 14). The upper limit prestressing is calculated to be 332 N/mm^2 by Eq. (12) (332/1251 = 26.6% of the tensile strength for BFRP rod) which is 2.46 times higher than that without BFRP sheet (135 N/mm^2). Here, the value of G_f is 0.87 N/mm referencing to the past experimental research [22] in which the BFRP sheet is bonded by the epoxy resin. While the measured value for the stretch adhesion test is 326 N/mm^2 (326/1251 = 26.1% of the tensile strength for BFRP rod) which is very closer to the theoretical value. The correctness and the applicability of the formula presented in this paper are verified once again.

Conclusions

In this paper, the BFRP rod is tensioned and bonded to the surface of the concrete beams which is used as a method for evaluate the special shearing stress generated at the adhesive end portion. Through the prestressed import test and the stretch adhesion test at both ends, the shear stress at the bonding end is compared by theory and experiment. In addition, the adhesive width is widened by bonding the edge of the adhesive around the BFRP sheet which increases the adhesion. The following conclusions are drawn from the above studies:

(1) The shear stress $\tau(x)$ produced at the bonding end in the stretch adhesion test theoretically indicates that using the stretch adhesion test at both ends can evaluate the shear stress produced at the bonding end in prestressed import test.
(2) The theoretical formula for calculating the maximum shear stress of the bonding end is proposed according to the stretch adhesion test at both ends. By compared with the experimental results, the accuracy and applicability of the theoretical formula are verified. When the safety factor is 1, the maximum shear stress calculated by the proposed formula is consistent with the maximum shear stress obtained by the prestressed import test, which proves the general applicability of the theoretical formula proposed by this paper.
(3) Prior to bonding the BFRP rod, pasting BFRP sheet, the bonding width can be relaxed and the maximum shear stress can be increased by 2.46 times. Moreover, the maximum shear stress calculated by the theoretical formula proposed in this paper is consistent with the experimental value.

Acknowledgements

The writers are grateful for the Science Foundation for Young Scholars of Wuhan Institute of Technology (Q201603), the National Nature Science Foundation of China (51408443) and the Hubei Chenguang Talented Youth Development Foundation. The writers also very much appreciate the Meijo University.

References

[1] Sim J, Park C, Moon DY. Characteristics of basalt fiber as a strengthening material for concrete structures. Compos B 2005;36(6/7):504–12.
[2] Wu Gang, Dong Zhigiang, Wang Xin, Wu Zhishen. Experimental study on the durability of BFRP bars embedded in concretes. J Southeast Univ (English Edition) 2014;30(3):323–9.
[3] Dong Zhigiang, Wang Xin, Wu Zhishen. Prediction of long-term performance and durability of BFRP bars under the combined effect of sustained load and corrosive solutions. J Compos Constr 2015;19(3). 04014058.
[4] Zhao XL, Raman Singh RK, Al-Saadi. Tests on seawater and sea sand concrete-filled CFRP, BFRP and stainless steel tubular stub columns. Thin-walled Struct 2016;108:163–84.
[5] Pawlowski D, Szumigala M. Theoretical and numerical study of the flexural behavior of BFRP RC beams. Eng Trans 2016;64(2):213–23.
[6] Jiang Shaofei, Zeng Xinggui, Shen Sheng, Xu Xincheng. Experimental studies on the seismic behavior of earthquake-damaged circular bridge columns repaired by using combination of near-surface-mounted BFRP bars with external BFRP sheets jacketing. Eng Struct 2016;106:317–31.
[7] Cheng Haigen, Tian Qin, Shang Jingmiao, Lu Dinkun. Experimental research on the flexural capacity of reinforced concrete beams reinforced with BFRP. Open Constr Build Technol 2015;9(1):277–86.
[8] Ouyang Lijun, Gao Wanyang, Zhen Bin, Lu Zhoudao. Seismic retrofit of square reinforced concrete columns using basalt and carbon fiber-reinforced polymer sheets: a comparative study. Compos Struct 2017;162:294–307.
[9] Lu Zhongyu, Xie Jianhe, Zhang Huan, Li Jianglin. Long-term durability of basalt fiber-reinforced polymer (BFRP) sheets and the epoxy resin matrix under a wet-dry cyclic condition in a chloride-containing environment. Polymers 2017;9(12):652.
[10] Qin Lihui, Wang Zonglin, Wu He, Zhang Lan. Experimental study of flexural behavior of RC beams strengthened with BFRP sheets. Key Eng Mater 2013;540:119–29.
[11] Ibrahim AMA, Wu Zhishen, Fahmy MFM, Kamal D. Experimental study on cyclic response of concrete bridge columns reinforced by steel and basalt FRP reinforcement. J Compos Constr 2016;20(3):04015062.
[12] Wu Gang, Dong Zhiqiang, Wang Xin. Prediction of long-term performance and durability of BFRP bars under the combined effect of sustained load and corrosive solutions. J Compos Constr 2014;19(3):04014058.
[13] Anandakumar R, Selvamony C, Seeni A. Performance of BFRP retrofitted RCC piles subjected to axial loads. Adv Mater Sci Eng 2015;2014:1–9.
[14] Yao LZ, Wu G. Fiber-element modeling for seismic performance of square RC bridge columns retrofitted with NSM BFRP bars and/or BFRP sheet confinement. J Compos Constr 2016;20(4):04016001.
[15] Wu ZS, Niu HD. Study on debonding failure load of RC beams strengthened with FRP sheets. J Struct Eng 2000;46A:1431–41.
[16] Niu HD, Wu ZS. Interfacial shear transfer in strengthened structure with FRP prestressing technique, CJCJCC-5. Kunming 2002:71–80.
[17] Wu G, Zhang L, Zhang JF, Hui D. Experimental study on the fire resistance of RC beams strengthened with near-surface-mounted high-Tg BFRP bars. Composites Part B 2014;60:680–7.
[18] Lv ZY, Xian GJ. Combined effects of sustained tensile loading and elevated temperatures on the mechanical properties of pultruded BFRP plates. Constr Build Mater 2017;150:310–20.
[19] Li YY, Wang YL, Ou JP. Mechanical behavior of BFRP-steel composite plate under axial tension. Polymers 2014;6(6):1862–76.
[20] Zhang P, Zhu Hong, Chen Q, Meng SP, Liu XY. Experimental analysis of shear performance of wet-bonding interface between FRP plate and concrete. Tumu Jianzhu yu Huanjing Gongcheng 2011;33(3):74–9. [in Chinese].
[21] Wu ZS, Yuan H, Niu HD. Stress transfer and fracture propagation in different kinds of adhesive joints. J Eng Mech, ASCE 2002;128(5):562–73.
[22] Iwashita K, Sato D, Baba S, Matsumoto N. Bond behaviour of BFRP sheets for concrete structure. In: *Proceedings of the Japan Concrete Institute*. 2014;36(1):1912–7 [in Japanese].